Modeling and simulation for dye-sensitized solar cells

Virginia Yong, Seng-Tiong Ho, and Robert P. H. Chang

Citation: Applied Physics Letters **92**, 143506 (2008); doi: 10.1063/1.2908204
View online: http://dx.doi.org/10.1063/1.2908204
View Table of Contents: http://scitation.aip.org/content/aip/journal/apl/92/14?ver=pdfcov
Published by the AIP Publishing

Modeling and simulation for dye-sensitized solar cells

Virginia Yong, Seng-Tiong Ho, and Robert P. H. Chang[a)]
Materials Research Institute, Materials Science and Engineering Department, and Electrical Engineering and Computer Science Department, Northwestern University, Evanston, Illinois 60208, USA

(Received 6 December 2007; accepted 3 March 2008; published online 11 April 2008)

We developed an equivalent circuit for dye-sensitized solar cells, which provides a more accurate presentation and a better fit to the experimental *I-V* curves and Nyquist plots than earlier literature results, as verified by simulation. A simple expression for the estimation of the Warburg coefficient from the experimental Nyquist plot is also proposed in this letter. The simulated *I-V* curves and Nyquist plots are in good agreement with the experimental data. The interfacial charge transfer and recombination losses at the oxide/dye/electrolyte interface are found to be the most influential factor on the overall conversion efficiency. © *2008 American Institute of Physics*.
[DOI: 10.1063/1.2908204]

Dye-sensitized solar cell (DSSC), invented by O'Regan and Gratzel,[1] reached energy conversion efficiencies of 11% (Refs. 2–4) under standard conditions (AM1.5G, 100 mW/cm^2 at 298 K) rendering it a credible alternative to conventional *p-n* junction photovoltaic devices. *cis*-di(thiocyanato)bis(2,2′-bipyridyl-4,4′-dicarboxylate) ruthenium(II), coded as N719 or N3 dye depending on whether it contains two or four protons, was found to be an outstanding solar light absorber and charge-transfer sensitizer.[5] The most widely used *n*-type oxide material for charge collection and conduction is TiO_2, although other wide-band-gap semiconductor oxides such as ZnO, SnO_2, or Nb_2O_5 have also been explored.[6–8] Photoexcitation of the sensitizer results in the charge separation at the interface and the electron injection from the dye into the conduction band of the oxide. The dye is regenerated by electron donation from the electrolyte, usually an organic solvent containing a redox system, such as the iodide/triiodide (I^-/I_3^-) couple. The I^- is regenerated by the reduction of I_3^- at the counter electrode, with the circuit being completed via electron migration through the external load. The standard cell construction is fluorine-doped tin oxide (FTO) glass | TiO_2—N719 dye | electrolyte with I^-/I_3^- redox couple | platinum-sputtered FTO.[2]

Electrochemical impedance spectroscopy (EIS) is a steady state method of measuring the current response to the application of an ac voltage as a function of the frequency to study the kinetics of electrochemical and photoelectrochemical processes. In the Nyquist plots, the respective electrochemical steps with different time constants are represented by the semicircles. For DSSC, the Nyquist plot typically features three or four semicircles,[9–11] which indicates that at least three to four photoelectrochemical processes are predominant in the photovoltage drop. Although extensive efforts have undertaken to visualize an equivalent circuit to signify the photoelectrochemical processes in DSSCs,[10,12,13] a verification of the validation of the proposed equivalent circuits, both dc and ac represented by experimental current-voltage (*I-V*) curves and Nyquist plots, is still unavailable to date. We performed simulation to examine the equivalent circuits reported in the literature and could not confirm their validation. We find that the transmission line and ladder circuit normally used as an equivalent circuit for modeling DSSCs[10,12] does not exhibit a diode characteristic and is not able to conform to the typical *I-V* curves [Figs. 1(a) and 1(b)]. Han *et al.* proposed a simple equivalent circuit model for DSSC similar to that of a conventional *pn*-junction solar cell.[13] However, we find that the model of Han *et al.* exhibits two semicircles only in the Nyquist plot instead of the three or four semicircles experimentally observed and is completely out of scale when we tried to fit the experimental *I-V* curve and Nyquist plot of Gratzel cells extracted from the literature[2,10] [Figs. 1(c) and 1(d)]. This letter proposes an equivalent circuit model interpreting the frequency response in terms of the fundamental electronic and ionic processes occurring in the photovoltaic device. The *I-V* curves and Nyquist plots are simulated from the impedance parameters, allowing a verification of the equivalent circuit model and a delineation of the contribution of different photoelectrochemical processes to the overall conversion efficiency.

A standard DSSC typically contains three interfaces formed by FTO/TiO_2, TiO_2/dye/electrolyte, and electrolyte/Pt-FTO. An equivalent circuit model is shown in Fig. 2. The interfacial charge transfer at the TiO_2/dye/electrolyte is represented by a rectifying diode (D_i) and a double-layer capacitance (C_i). A recombination diode D_r with an ideality factor generally considered as equal to 2 (Refs. 14 and 15) is employed to denote the interfacial charge recombination losses to both the dye cation and the redox electrolyte. A

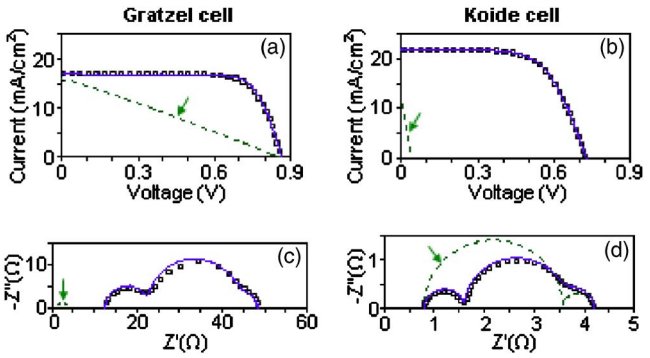

FIG. 1. (Color online) Open squares: experimental data of Gratzel and Koide solar cells extracted from the literature, Refs. 2, 10, and 11. Dotted lines (pointed by arrows): simulation of earlier literature models, Refs. 10, 12, and 13. Solid lines: simulated *I-V* curves and Nyquist plots based on the equivalent circuit model in Fig. 2.

a)Electronic mail: r-chang@northwestern.edu.

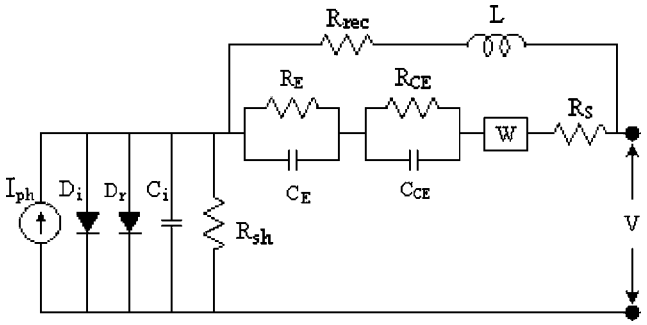

FIG. 2. An equivalent circuit model of DSSCs.

shunt resistance R_{sh} takes into account all parallel resistive losses across the photovoltaic device including leakage current. The photogenerated current I_{ph} is in parallel with the rectifying diode. An inductive recombination pathway as a result of a charge-transfer current[16] is incorporated into the circuit, consisting of a recombination resistance (R_{rec}) in series with an inductor (L).[17] The charge-transfer resistance and interfacial capacitance at the FTO electrode and electrolyte/Pt-FTO interface are represented by R_E and C_E, and R_{CE} and C_{CE}, respectively. The Nernst diffusion of the carrier transport by ions within the electrolyte is denoted by the Warburg impedance (W).[18] A resistance element R_S designates the bulk and contact resistive losses present in a practical DSSC, such as the sheet resistance of the FTO glass.

The corresponding I-V characteristic based on the equivalent circuit model in Fig. 2 is described by the following equations:[15,18,19]

$$I = I_{ph} - I_i\left\{\exp\left[\frac{q(V+IZ)}{k_BT}\right]-1\right\} - I_r\left\{\exp\left[\frac{q(V+IZ)}{2k_BT}\right]-1\right\} - (V+IZ)(j\omega C_i + 1/R_{sh}), \quad (1)$$

$$I_{ph} = \int qF(\lambda)[1-r(\lambda)]\mathrm{IPCE}(\lambda)d\lambda = \int qF(\lambda)\Phi(\lambda)d\lambda, \quad (2)$$

$$Z = \frac{1}{1/(R_{rec}+j\omega L)+1/Z_S}, \quad (3)$$

$$Z_S = \frac{1}{j\omega C_E + 1/R_E} + \frac{1}{j\omega C_{CE}+1/R_{CE}} + W + R_S, \quad (4)$$

$$W = \sigma\omega^{-1/2}(1-j), \quad (5)$$

where I_i and I_r are the saturation current density of the rectifying and recombination diodes, respectively, k_B is the Boltzmann constant, T is the absolute temperature, q is the electron charge, ω is the angular frequency, σ is the Warburg coefficient, $F(\lambda)$ and IPCE(λ) are the incident photon flux density and the incident photon-to-current conversion efficiency at wavelength λ, respectively, $r(\lambda)$ is the incident light losses due to the light absorption and reflection by the FTO glass, and $\Phi(\lambda)$ is the quantum yield.

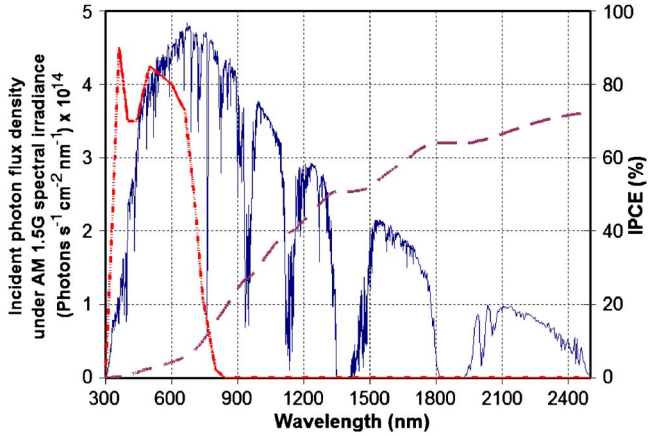

FIG. 3. (Color online) Simulated incident photon flux density and IPCE versus excitation wavelength. Solid line: incident photon flux density under AM1.5G spectral irradiance. Dotted line: IPCE of a typical state-of-the-art DSSC. Dashed line: cumulative quantum yield loss in percentage.

For highly efficient DSSCs at AM1.5G, short-circuit photocurrent densities (I_{sc}) ranging from 16 to 22 mA/cm^2 are reached, while open-circuit voltage (V_{oc}) is 0.7–0.86 V and fill factor (FF) values are 0.65–0.8.[2] Figure 3 shows the IPCE of a typical state-of-the-art DSSC,[2] and the simulated $F(\lambda)$ and $1-\Phi(\lambda)$. The cumulative quantum yield loss is calculated as $\int_0^\lambda F(\lambda)[1-\Phi(\lambda)]d\lambda / \int_0^\infty F(\lambda)d\lambda$. I_{ph} can be obtained using Eq. (2) based on the data in Fig. 3, which is in good agreement with the typical I_{ph} ($\sim$20 mA/cm^2) for an efficient solar cell. Figure 1 shows the simulated I-V curves and Nyquist plots of highly efficient DSSCs, with superimposed experimental data extracted from the literature.[2,10,11] Impedance spectra are simulated over a frequency range of $0.01-10^6$ Hz with an ac amplitude of 10 mV. The values of model parameters used in the simulation are summarized in Table I. The shunt resistance R_{sh} can be estimated from the slope of the I-V curve at the short-circuit current point, which is typically of the order of 10^3 Ω for a highly efficient solar cell. I_i and I_r are found to be of the orders of 10^{-15} and 10^{-10} A/cm^2, respectively. The inductor L (negative capacitance) is 10–100 H.[17] The double-layer capacitance C_i is determined to be of the order of 10 F. The large capacitance value at the TiO_2/dye/electrolyte interface (C_i) is likely resulted from the large surface area of the nanocrystalline TiO_2 structure. The length between the intercepts at the real axis corresponds to the charge-transfer resistance (R_{ct}) of the

TABLE I. Summary of the values of model parameters used in simulated I-V curves and Nyquist plots in Fig. 1.

	I_{ph} (mA/cm^2)	I_i (A/cm^2)	I_r (A/cm^2)	C_i (F)	R_{sh} (Ω)	R_{rec} (Ω)
Gratzel	16.9	0.4×10^{-16}	1.4×10^{-10}	10	3000	4.2
Koide	21.9	1×10^{-15}	1.5×10^{-8}	10	3000	4.2
	R_E (Ω)	C_E (mF)	R_{CE} (Ω)	C_{CE} (μF)	σ (Ω s$^{-1/2}$)	R_S (Ω)
Gratzel	21.7	0.8	9.8	19	4.2	12.6
Koide	2	0.7	0.8	5	1.9	0.8

component. The double-layer capacitance (C_{dl}) is determined from the characteristic frequency, $C_{dl}=(R_{ct}\,\omega_{max})^{-1}$.[19] The resistance elements R_{rec}, R_E, R_{CE}, and R_S are typically several ohms for a highly efficient solar cell. The interfacial capacitances C_E and C_{CE} are of the orders of 1 mF and 1 μF, respectively.

In DSSC, the standard electrolyte consists of the I^-/I_3^- redox couple dissolved in acetonitrile and the reaction scheme is $3I^- \rightleftharpoons I_3^- + 2e^-$, with the I^- ion reduces the dye molecule and the oxidized redox species I_3^- diffuses to the Pt-FTO counter electrode. The concentration of I_3^- ions in a standard DSSC is one order of magnitude smaller than that of I^-.[20] Therefore, the diffusion of the I_3^- ions through the TiO_2 network and finally to the counter electrode may be a limiting factor for the overall efficiency of the DSSCs. Kron *et al.* investigated the diffusion limitations due to I_3^- transport and showed that at voltages below 0.3 V, electronic transport is dominated by the catalytic reaction at the Pt/electrolyte interface whereas above ~0.4 V current flow is limited by diffusion of I_3^- through the nanoporous TiO_2 network.[21] In EIS, the Nernst diffusion of the carrier transport by ions within the electrolyte is denoted by the Warburg impedance (W).[18] As the low-frequency region on the Nyquist plot of DSSC features the shape of a semicircular arc, we approximate W with a parallel RC circuit (a resistor R_D and a capacitor C_D) and equate it to W in Eq. (5), hence $W=\sigma\omega^{-1/2}(1-j)\approx 1/(j\omega C_D+1/R_D)\Rightarrow\sigma\approx\omega^{1/2}R_D/(1-j)(1+j\omega R_D C_D)$. Using the approximation $\omega\approx\omega_{max}=(R_D C_D)^{-1}$, therefore

$$\sigma \approx \frac{R_D}{2\sqrt{R_D C_D}}, \tag{6}$$

where R_D and C_D can be estimated from the diameter of the low frequency arc (in the millihertz range) in the Nyquist plot and the characteristic frequency using the expression $C_D=(R_D\,\omega_{max})^{-1}$, respectively. From the Nyquist plot of high-efficiency DSSCs,[10,11] we determine R_D and C_D to be ~2.5 Ω and 0.05 F, respectively. From Eq. (6), the estimated σ is found to be of the order of 1 $\Omega\,s^{-1/2}$. This corresponds to a diffusion constant of I_3^- ($D_{I_3^-}$) of the order of 1×10^{-5} $cm^2\,s^{-1}$ calculated from $\sigma=RT/n^2F^2A\sqrt{2}[1/C_{I_3^-}(D_{I_3^-})^{1/2}+1/C_{I^-}(D_{I^-})^{1/2}]$ (Ref. 18) by the estimated σ according to Eq. (6). R is the ideal gas constant, T is the absolute temperature, n is the number of electrons transferred (here $n=2$ considering the two-electron reaction scheme of $3I^- \rightleftharpoons I_3^- + 2e^-$), F is Faraday's constant, and A is the electrode area. $C_{I_3^-}$ and C_{I^-} are the concentration of I_3^- and I^-, respectively, with $A=1$ cm^2 and $C_{I_3^-}=50$ mM for a standard DSSC, and $C_{I^-}\gg C_{I_3^-}$.[20,22] $D_{I_3^-}$ and D_{I^-} are the diffusion constant of I_3^- and I^-, respectively, and $D_{I^-}\approx 1.2D_{I_3^-}$.[22] The $D_{I_3^-}$ value calculated from our estimated σ is in good agreement with the diffusion constant of I_3^- experimentally obtained.[21]

The influence of each parameter on the overall conversion efficiency is simulated. For highly efficient DSSCs, I_i and I_r appear to have the largest influence on the overall conversion efficiency, more prominent for the recombination losses (Fig. 4). However, the effect of resistive elements starts becoming dominant when the series resistance is getting larger, especially detrimental to the fill factor.

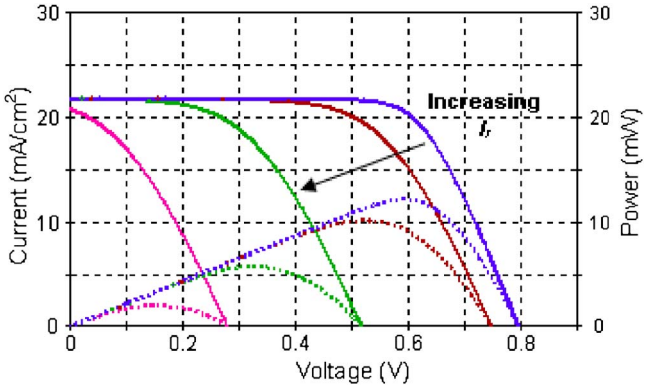

FIG. 4. (Color online) Simulated *I-V* curves based on the equivalent circuit model in Fig. 2 showing the effect of recombination losses at the TiO_2/dye/electrolyte interface represented by the changes (10^{-10}, 10^{-8}, 10^{-6}, and 10^{-4} A/cm^2) in I_r, the saturation current density of the recombination diode. Solid lines: current. Dotted lines: power.

Our work will help understand the device physics of DSSCs, predict the efficiency, guide the device optimization, and facilitate the development of future structures and technological processes.

The authors would like to thank the National Science Foundation and Department of Energy for financial support.

[1] B. O'Regan and M. Gratzel, Nature (London) **353**, 737 (1991).
[2] M. Gratzel, Inorg. Chem. **44**, 6841 (2005).
[3] Y. Chiba, A. Islam, Y. Watanabe, R. Komiya, N. Koide, and L. Han, Jpn. J. Appl. Phys., Part 2 **45**, L638 (2006).
[4] M. Wei, Y. Konishi, H. Zhou, M. Yanagida, H. Sugihara, and H. Arakawa, J. Mater. Chem. **16**, 1287 (2006).
[5] Md. K. Nazeeruddin, R. Humphry-Baker, P. Liska, and M. Gratzel, J. Phys. Chem. B **107**, 8981 (2003).
[6] M. Quintana, T. Edvinsson, A. Hagfeldt, and G. Boschloo, J. Phys. Chem. C **111**, 1035 (2007).
[7] A. Green, E. Palomares, S. Haque, J. Kroon, and J. Durrant, J. Phys. Chem. B **109**, 12525 (2005).
[8] F. Lenzmann, J. Krueger, S. Burnside, K. Brooks, M. Gratzel, D. Gal, S. Ruhle, and D. Cahen, J. Phys. Chem. B **105**, 6347 (2001).
[9] T. Hoshikawa, R. Kikuchi, K. Sasaki, and K. Eguchi, Electrochemistry (Tokyo, Jpn.) **70**, 675 (2002).
[10] Q. Wang, J. Moser, and M. Gratzel, J. Phys. Chem. B **109**, 14945 (2005).
[11] N. Koide, A. Islam, Y. Chiba, and L. Han, J. Photochem. Photobiol., A **182**, 296 (2006).
[12] Q. Wang, S. Ito, M. Gratzel, F. Fabregat-Santiago, I. Mora-Sero, J. Bisquert, T. Bessho, and H. Imai, J. Phys. Chem. B **110**, 25210 (2006).
[13] L. Han, N. Koide, Y. Chiba, A. Islam, R. Komiya, N. Fuke, A. Fukui, and R. Yamanaka, Appl. Phys. Lett. **86**, 213501 (2005).
[14] A. Luque and S. Hegedus, *Handbook of Photovoltaic Science and Engineering* (Wiley, Hoboken, 2003).
[15] T. Markvart and L. Castaner, *Solar Cells: Materials, Manufacture and Operation* (Elsevier Science, Oxford, 2005).
[16] A. Sadkowski, J. Electroanal. Chem. **465**, 119 (1999).
[17] I. Mora-Sero, J. Bisquert, F. Fabregat-Santiago, G. Garcia-Belmonte, G. Zoppi, K. Durose, Y. Proskuryakov, I. Oja, A. Belaidi, T. Dittrich, R. Tena-Zaera, A. Katty, C. Levy-Clement, V. Barrioz, and S. Irvine, Nano Lett. **6**, 640 (2006).
[18] E. Barsoukov and J. R. Macdonald, *Impedance Spectroscopy: Theory, Experiment, and Applications* (Wiley-Interscience, Hoboken, 2005).
[19] P. J. Gellings and H. J. Bouwmeester, *Handbook of Solid State Electrochemistry* (CRC, Boca Raton, 1997).
[20] N. Papageorgiou, Y. Athanassov, M. Armand, P. Bonhote, H. Pettersson, A. Azam, and M. Gratzel, J. Electrochem. Soc. **143**, 3099 (1996).
[21] G. Kron, U. Rau, M. Durr, T. Miteva, G. Nelles, A. Yasuda, and J. H. Werner, Electrochem. Solid-State Lett. **6**, E11 (2003).
[22] T. Oda, S. Tanaka, and S. Hayase, Sol. Energy Mater. Sol. Cells **90**, 2696 (2006).